THE ASTROPHYSICAL JOURNAL, 408:57–70, 1993 May 1

COMPRESSIVE TIDAL HEATING OF A DISK GALAXY IN A RICH CLUSTER

MONICA VALLURI
Joint Astronomy Program, Department of Physics, Indian Institute of Science, Bangalore 560012, India
Received 1992 May 20; accepted 1992 October 21

ABSTRACT

The effects of the mean tidal field of a cluster of galaxies on the internal dynamics of a disk galaxy traveling through it are studied in the restricted three-body framework. In the model adopted the galaxy experiences a tidal field that is compressive within the core of the cluster. The effect of the cluster tidal field on the disk galaxy in this region of the cluster resembles the phenomenon of compressive shocking of globular clusters by the Galactic disk.

A disk parallel to its orbital plane in the cluster develops a transient, two-armed spiral pattern. A disk which is perpendicular or inclined to the orbital plane is transiently compressed and the originally circular disk is deformed into an ellipse. Also, the planar random velocities of all components in the disk increase after the galaxy passes through the core of the cluster. The low-velocity dispersion (5–10 km s^{-1}) gas clouds experience a relatively larger increase in random velocity than the hotter stellar components (20–35 km s^{-1}). A strong tidal field can increase the planar random velocities of all particles to between 50 and 70 km s^{-1}.

The increase in planar velocities results in a strong anisotropy between the planar and vertical velocity dispersions. We argue that this will make the disk unstable to the "fire-hose instability" which leads to bending modes in the disk and which will thicken the disk slightly. The mean tidal fields in rich clusters were probably stronger during the epoch of cluster formation and relaxation than they are in present-day relaxed clusters. It is suggested that the activity in spiral galaxies in high redshift clusters (the Butcher-Oemler clusters) could have been triggered by these strong tidal fields.

Subject headings: galaxies: clustering — galaxies: evolution — galaxies: interactions — galaxies: kinematics and dynamics

1. INTRODUCTION

A variety of observations of galaxies in clusters indicate that the gas in these galaxies is strongly affected by the cluster environment. For instance, it is well known that spiral galaxies in clusters are H I-deficient as compared to isolated field spirals (e.g., Giovanelli & Haynes 1985). It is popularly believed that the ram pressure exerted on the interstellar medium (ISM) by the intracluster gas causes gas stripping (Gunn & Gott 1972).

In recent times it has been realized that the mean tidal field of the cluster potential may affect the internal dynamics of galaxies within it. Miller (1988) suggested that the cumulative effects of interactions between galaxies and the effect of the weak, but long-lived, tidal perturbation of the cluster potential can "shake-up" galaxies in clusters and lead to the formation of elliptical galaxies. Merritt (1984) showed that a spherical galaxy in a cluster could be tidally truncated to a radius of 30 h_{50}^{-1} kpc if it passed within a few core radii of the center of a Coma-like cluster. N-body simulations on a disk galaxy placed at a distance of 650 kpc from a point perturber with cluster mass (Byrd & Valtonen 1990) showed that it would develop a strong bar and a two-armed spiral feature followed by substantial gas infall to the center of the galaxy.

Here we present results of a study of the dynamical evolution of a disk galaxy as it falls into a cluster for the first time on a bound orbit with constant angular momentum. The problem is studied in the restricted three-body framework. The orbits of test particles in the galaxy are evolved in the combined fields of the galaxy and the cluster which are prescribed analytically. One drawback of the method is that the self-gravity of the disk particles is not considered, unlike in N-body simulations where the system evolves self-consistently. Nevertheless, this method can effectively complement N-body work since it has been shown (Toomre & Toomre 1972) that this method can reproduce the broad features of interacting galaxies fairly accurately. Second, since the computing power required is small one can scan the parameter space and identify regions of interest for future N-body studies. The aim of this study is to understand the basic dynamics of the interaction.

The mean tidal field is strongest within 2 core radii of the cluster center. For realistic parameters the time taken for the galaxy to cross this region is typically a few times 10^8 yr (for a cluster with a line-of-sight velocity dispersion $\simeq$1000 km s^{-1} and a core radius 250 h_{50}^{-1} kpc). This is comparable to the rotation time in the disk. Therefore, the encounter is neither impulsive nor adiabatic and a time-dependent study is essential. This model ensures that the tidal field experienced by the galaxy changes gradually along its orbit within the cluster. Other workers (Miller & Smith 1982; Byrd & Valtonen 1990) have studied the response of a galaxy at a fixed distance from the cluster center to an impulsive tidal field which is suddenly "turned on."

The cluster tidal field is purely compressive within 1 core radius of the cluster center (§ 2.1). This must be contrasted with the tidal fields encountered in galaxy-galaxy interactions which are disruptive along the line joining the two galaxies. The galaxy travels through the cluster on a bound and fairly radial orbit as discussed in § 2.2. In § 2.3 the equations of motion of the particles in the disk in the combined field of the disk and the cluster tidal field are obtained and the conditions under which they are solved are described. The orientation of the plane of the disk relative to its orbital plane is an additional parameter in the problem and four distinct orientations are discussed. The velocities and distributions of particles in the

disk are changed as a result of the encounter and the dependence of these changes on various parameters in the problem are discussed (§ 3). In § 4 we briefly discuss a few possible stellar dynamical consequences of the tidal interaction based on the numerical results. In § 5 the main results from this work are summarized.

2. THE MODEL

The cluster is modeled by the modified Hubble potential (also called the analytic King profile). It has a density distribution,

$$\rho(r) = \frac{\rho_0}{[1 + (r/a)^2]^{3/2}}, \tag{1a}$$

where a is the core radius and ρ_0 is the central density, which are related to the line-of-sight velocity dispersion σ_{cl} and the core radius via the relation

$$\rho_0 = \frac{9\sigma_{cl}^2}{4\pi G a^2}, \tag{1b}$$

(see Binney & Tremaine 1987, hereafter BT). King (1972) showed that the luminosity distribution in the Coma Cluster was well-fitted by this profile. The luminosity distributions of several other clusters have been successfully fitted by this distribution truncated at some radius (cf. Sarazin 1986). The King model is known to provide a good fit to the data within 3–4 core radii. Since this is also the region within which the effects of the tidal field are strongest (see § 2.1), the fact that the mass of this potential diverges will not affect the results.

For the most part, the disk galaxy is modeled by a three-dimensional, highly flattened, logarithmic potential, with R and z in units of kpc,

$$\Phi_g(R, z) = \frac{v_c^2}{2} \ln\left[R_c^2 + R^2 + \left(\frac{z}{q}\right)^2\right], \tag{2}$$

where v_c is the asymptotic circular (flat) rotation velocity, R_c is a softening parameter, and q is a flattening parameter. This potential exhibits some features of observed disk galaxies such as a flat rotation curve (BT).

In the following section the tidal field terms at an arbitrary point in a general spherical potential are obtained and these are then used to derive the expressions for the tidal field terms for the cluster potential corresponding to the density distribution in equation (1).

2.1. *The Tidal Field of the Cluster Potential*

The tidal field terms at an arbitrary point in a potential are best obtained in Cartesian coordinates (X_1, X_2, X_3), with origin at the cluster center. The gratitational field at a point (X_{10}, X_{20}, X_{30}) due to the cluster potential $\Psi(X_1, X_2, X_3)$ is

$$\boldsymbol{F}(X_1, X_2, X_3) = -\nabla\Psi = -\sum_j \frac{\partial\Psi}{\partial X_j}\hat{\boldsymbol{e}}_{x_j}.$$

Taylor expanding $\boldsymbol{F}$ about the point (X_{10}, X_{20}, X_{30}) we have

$$\boldsymbol{F}(X_1, X_2, X_3) = \boldsymbol{F}(X_{10}, X_{20}, X_{30}) + \sum_i \left.\frac{\partial \boldsymbol{F}}{\partial X_i}\right|_0 \delta X_i + O[(\delta X_i \delta X_j)] + O[(\delta X_i)^2]. \tag{3}$$

For the tidal field we retain terms to first order in the Taylor expansion of the force. We can neglect asymmetric terms of the form $(\delta X_i \delta X_j)$ if the impact parameter of the galaxy with the cluster center is greater than 5 galaxy radii. We therefore select only those galaxy orbits that satisfy this condition (§ 2.2). We define $\delta X_i = X_i - X_{i0} = x_i$. This is used to define a Cartesian coordinate system (x_1, x_2, x_3), with origin at the galaxy center (X_{10}, X_{20}, X_{30}), and with x_i parallel to X_i for each i (see Fig. 1). The tidal field terms in the coordinate system (x_1, x_2, x_3) are then

$$T_{x_j} = -\left[\sum_i \left.\frac{\partial^2\Psi}{\partial X_i \partial X_j}\right|_0 x_i\right]\hat{\boldsymbol{e}}_{x_j}. \tag{4}$$

In spherical polar coordinates the potential for the density distribution in equation (1) is

$$\Psi(r) = \frac{-4\pi G\rho_0 a^3}{r}\left\{\ln\left[\left(\frac{r}{a}\right) + \sqrt{1 + \left(\frac{r}{a}\right)^2}\right]\right\}. \tag{5}$$

We make the substitution $X_1^2 + X_2^2 + X_3^2 = r^2$ and define the average density within the radius r as

$$\bar{\rho}(r) = \frac{3M(r)}{4\pi r^3}, \tag{6}$$

where $M(r)$ is the mass within the radius r. Differentiating twice we get

$$\frac{\partial^2\Psi}{\partial X_i \partial X_j} = \frac{4\pi G}{3}\left\{\delta_{ij}\bar{\rho}(r) + \frac{3X_i X_j}{r^2}[\rho(r) - \bar{\rho}(r)]\right\}. \tag{7}$$

This equation gives the tidal field terms in Cartesian coordinates, with ρ and $\bar{\rho}$ expressed as functions of the radial coordinate alone, since the cluster potential itself is spherically symmetric.

For a galaxy that is stationary at a point on the X_1-axis or is moving along this axis, $X_{10} = r$, $X_{20} = 0 = X_{30}$. In this case the tidal field terms become

$$T_{x_1} = \frac{4\pi G}{3}(2\bar{\rho} - 3\rho)x_1\hat{\boldsymbol{e}}_{x_1}; \tag{8a}$$

$$T_{x_2} = \frac{-4\pi G}{3}\bar{\rho}x_2\hat{\boldsymbol{e}}_{x_2}; \tag{8b}$$

$$T_{x_3} = \frac{-4\pi G}{3}\bar{\rho}x_3\hat{\boldsymbol{e}}_{x_3}. \tag{8c}$$

These are similar to the expressions obtained by Cowsik & Ghosh (1987).

For a galaxy on a nonradial orbit in the X_1–X_2 plane, which is the situation under consideration, $X_{30} = 0$ and $X_{10}^2 + X_{20}^2 = r^2$. Without loss of generality we can let the pericenter lie on the X_1-axis (see Fig. 1). The tidal field terms for this situation can also be obtained by performing a simple rotational transformation through an angle $\psi = \tan^{-1}(X_{20}/X_{10})$ on the expressions in equation (8) at each point (r, ψ) in the galaxy's orbit. In our calculations we use equations (8) and suitably transform them.

By substituting expressions for $\rho(r)$ and $\bar{\rho}(r)$ from equations (1) and (6) respectively, into equation (8) one can plot the cluster tidal field strengths as functions of the distance from the cluster center. In Figure 2 we plot (T_{x_1}/x_1) and $(T_{x_2}/x_2) = (T_{x_3}/x_3)$ (eq. [8]) as functions of (r/a). It can be seen from the figure that the values of the force terms are negative, or compressive, for (r/a) less than one core radius, but beyond this

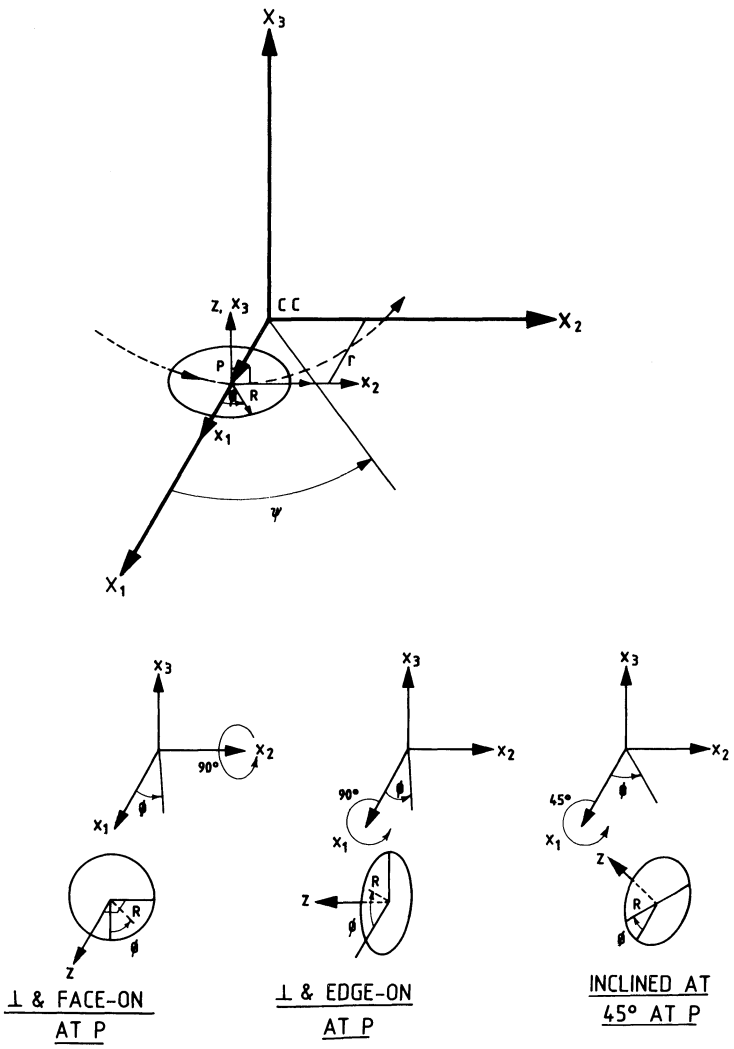

FIG. 1.—Geometry of the problem. Dashed line indicates the orbit of the galaxy in the X_1–X_2 plane. CC is the cluster center, and P indicates the pericenter point in the orbit. The orientation of axes are chosen so that P lies on the X_1-axis. Rotational transformations for the cases when the disk is not parallel to the orbital plane are made as indicated in the figures.

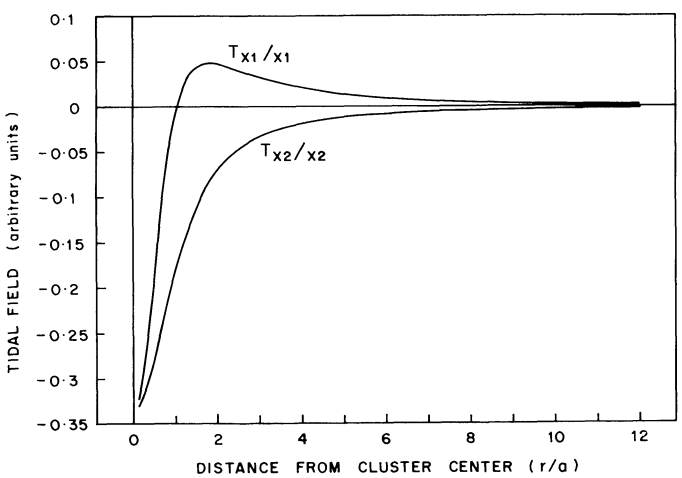

FIG. 2.—Tidal field strength per unit length, T_{x_1}/x_1 and $T_{x_2}/x_2 = T_{x_3}/x_3$, in arbitrary units plotted as functions of the distance from the cluster center in units of core radii a.

distance the component along the X_1-axis is positive or disruptive.

In deriving these expressions we have assumed that the dark matter in the cluster is smoothly distributed. If the local contribution of the dark matter of the cluster to the galaxy potential is greater than the disruptive force due to the cluster mass internal to the radius at which the galaxy is located, the force is compressive. Thus a galaxy passing through the core of the cluster will experience a compressive tidal force. This is reminiscent of the compressive tidal shocking of a globular cluster passing through the disk of the Galaxy (Ostriker, Spitzer, & Chevalier 1971) or through the Galactic bulge (Ostriker, Binney, & Saha 1989). Contrast this with tidal forces in galaxy-galaxy encounters which are disruptive along the direction vector between the galaxy centers and compressive in two orthogonal directions.

2.2. *Orbit of the Galaxy in the Cluster*

From the CfA Redshift Survey of Virgo Cluster galaxies, Huchra (1984) showed that while the elliptical and S0 galaxies

had a more or less Gaussian distribution in velocities, the spirals, on the other hand had a fairly uniform distribution with a "standard deviation" that was $2^{1/2}$ times that of the early-type population. This has been observed in several other clusters and this fact has been frequently used (Tammann & Binggeli 1987) to argue that while the early-type galaxies belong to an older, virialized population, the spirals are only just bound to the cluster potential and are falling in for the first time on radial orbits.

For simplicity we have assumed that the galaxy is on a two-body orbit in the cluster potential. A consideration of the clumpiness of the cluster potential and dynamical friction would result in a more complicated orbit.

It has been found (Bahcall 1975) that the core radii of the compact regular clusters are all very similar with an average value of $a = (0.25 \pm 0.04)\, h_{50}^{-1}$ Mpc. We use this value in most of the calculations. However, recent cluster gravitational lensing data seem to indicate that the core radius of the dark matter distribution is more like $0.1\ h_{50}^{-1}$ Mpc (Tyson, Valdes, & Wenk 1990), indicating a higher degree of central concentration than that deduced from the X-ray data. We perform calculations for five values of σ_{cl} and two values of a. The effects of varying these two parameters are discussed in § 3.

The energy and the angular momentum of the bound orbit are parametrized in units of a and σ_{cl}. The galaxy orbits had a constant value of $E = -1.5$ (in the units above). This gives an apocenter distance of ≈ 22 core radii. For a core radius of 250 kpc four values of L were used from $L = 1.6$ which gives an impact parameter of 0.45 core radii to $L = 5.0$ which gives an impact parameter of 1.5 core radii. For $a = 100$ kpc the orbit chosen had an angular momentum $L = 5.5$ with an impact parameter of 170 kpc. The effect of varying the orbital impact parameter is also discussed in § 3.

2.3. *Equations of Motion of Disk Particles*

For certain values of the parameters R_c and q, the logarithmic potential (eq. [2]) has properties which resemble those seen in a number of spiral galaxies. It is quadratic in R and z for small radii and has a flat rotation curve at large radii with asymptotic circular rotation velocity v_c. In the thin disk approximation ($q \ll 1$) the planar and vertical motions are decoupled. The planar rotation frequency, Ω, and the vertical frequency, ν, are related through

$$\nu^2 = \frac{\Omega^2}{q^2}\,. \tag{9}$$

We use the observed values of Ω and ν in the solar neighborhood to estimate q. In the solar neighborhood $\nu = (2\pi/6.6 \times 10^7)\ \mathrm{yr}^{-1}$ (from Oort's constant; see BT) and $\Omega = (2\pi/2.4 \times 10^8)\ \mathrm{yr}^{-1}$ (assuming the Sun to be at 8.5 kpc, and $v_c = 220\ \mathrm{km\ s}^{-1}$). Substituting in equation (9) we get a value of $q \sim 0.3$ in the solar neighborhood. We assume for convenience that this value is a constant across the disk. A typical "turnover radius" of 4 kpc for the rotation curve is obtained for a value of $R_c \sim 1.5$ kpc. The logarithmic potential with the above parameters is used for most of the calculations.

In § 3.3 the thin disk approximation is relaxed to explore the effects of the more spheroidal dark matter halo. A three-component Miyamoto-Nagai potential (Miyamoto & Nagai 1975) with a spheroid, a spheroid-disk, and a massive halo has been selected (Miyamoto, Satoh, & Ohashi 1980) to study the effects of the halo on disk particles. The results for this model are not very different from the results for the logarithmic potential and are discussed in detail in § 3.3.

The equations of motion for a particle in the galaxy under the combined force fields of the galaxy's potential in equation (2) and the cluster tidal field written in cylindrical polar coordinates are

$$\begin{aligned} \ddot{R} - R\dot{\varphi}^2 &= \frac{-\partial\Phi_g}{\partial R} + T_R(t)\,, \\ R\ddot{\varphi} + 2\dot{R}\dot{\varphi} &= T_\varphi(t)\,, \\ \ddot{z} &= \frac{-\partial\Phi_g}{\partial z} + T_z(t)\,, \end{aligned} \tag{10}$$

where R is the radial coordinate in the plane of the disk, φ is the azimuthal angle in the plane measured in the direction of rotation, and z is the normal to the disk (see Fig. 1). T_R, T_φ, T_z are the tidal field terms as functions of time, t, which are obtained by transforming each T_{x_i} in equation (8) suitably for each orientation of the disk to the orbital plane.

Equations (10) were solved numerically as an initial value problem with an adaptive step algorithm. The evolution of a three-dimensional thin disk, starting from an initially axisymmetric distribution of particles is studied. The orbits of particles are initially circular. Small initial radial and vertical perturbations result in epicyclic motion with frequency $\kappa = 2^{1/2}\Omega$ and vertical oscillation with frequency ν. It is assumed that the random motion of particles in the disk about the circular motion is entirely due to epicyclic and vertical oscillations which are decoupled. The choice of the initial amplitudes of the radial (epicyclic) velocity and the vertical oscillation velocity determines how "hot" the component under consideration is. If these velocities are initially zero the system is regarded as a "cold" disk. We study the response of various components of the disk, namely the low-velocity dispersion gas components (5–10 km s^{-1}), and the hotter stellar components (20–35 km s^{-1}) by suitably changing the initial radial and vertical velocity amplitudes. It must be pointed out here that although the expression "gas" is used frequently to mean the low random velocity component, no dissipation of energy occurs in this component as in the case of real gas clouds.

The observationally determined Schwarzschild ellipsoid in the solar neighborhood for gas and various stellar types (Mihalas & Binney 1981) is used to select initial random velocity amplitudes for some representative components (see Table 1). At the start of a simulation the ratio of the radial to tangential velocity dispersions is taken to be $2^{1/2}$ which is the expected ratio for a particle in epicyclic motion in a potential

TABLE 1

INITIAL RADIAL AND VERTICAL VELOCITY AMPLITUDES[a]

Component	v_r (km s^{-1})	v_z (km s^{-1})
H (gas)	5	5
H I (gas)	10	6
O–B stars	10	6
A stars	19	10
F–G stars	26	15
K–M stars	35	20

[a] Compiled from Mihalas & Binney 1981.

with a flat rotation curve (see BT). Each particle is also given a random phase in its epicyclic and vertical oscillation.

An additional parameter in the problem is the orientation of the plane of the galaxy relative to the plane of its orbit in the cluster. The assumption that the tidal torques on the galaxy do not alter its orientation during the encounter is likely to be a good one especially in the core region where the crossing time is small. We have performed simulations for four representative and distinct orientations of the disk (Fig. 1). The simplest case is when the plane of the disk is parallel to the plane of the orbit. There is no unique orientation for a disk perpendicular to the orbital plane. We therefore consider two special cases: in the first the disk is seen *edge-on* at the pericenter point by an observer located at the cluster center; and in the second the disk is seen *face-on* at pericenter. In the fourth case the disk is inclined at 45° to the plane of the orbit. This orientation is obtained by rotating a parallel disk through 45° anticlockwise about the radial vector from the pericenter to the cluster center. The expressions for T_R, T_φ, and T_z in equation (10) for these orientations of the disk are easily obtained by suitably transforming equation (8). Here we give only the expressions for the tidal force terms when the disk is parallel to the orbital plane.

$$T_R = R[\xi_2 \cos 2(\psi - \varphi) + \xi_1] , \tag{11a}$$

$$T_\varphi = -R[\xi_2 \sin 2(\psi - \varphi)] , \tag{11b}$$

$$T_z = z(\xi_2 - \xi_1) , \tag{11c}$$

where the quantities ξ_1 and ξ_2 are

$$\xi_1 = \frac{-4\pi G}{2}(\rho - \bar{\rho}) , \quad \xi_2 = \frac{-4\pi G}{6}(3\rho - \bar{\rho}) .$$

The angle ψ is the azimuthal angle in the orbital plane (with origin at cluster center) between the position of the galaxy at any point in the orbit and the pericenter position. It may be noted that ξ_1 and ξ_2, (which are functions of ρ and $\bar{\rho}$), and ψ are functions of time since they change along the galaxy's orbit. For this orientation of the disk it can be seen that the "tidal potential" has a cos $2(\psi - \varphi)$ dependence and is clearly bisymmetric in the plane of the disk. The consequences of the bisymmetry are discussed in § 3.2. Such a simple bisymmetry in the "tidal potential" does not exist for other orientations of the disk.

3. NUMERICAL RESULTS

In this section the numerical results and their dependence on various parameters in the model are discussed. The results for a "standard" set of parameters—a cluster core radius of 250 kpc, a velocity dispersion of 1000 km s^{-1}, an orbit with $E = -1.5$ and $L = 2.5$ (see § 2.2 for the definition of E and L)—are discussed first. The disk is parallel to the orbital plane. The disk is assumed to have an asymptotic circular velocity $v_c = 220$ km s^{-1}. The orbits of particles in the galaxy are evolved from a time when the galaxy is at a distance of ~12 core radii (or 3 Mpc) from the cluster center. From Figure 2 it is clear that the tidal forces at this distance are negligible and hence the forces are not "turned on" suddenly in our treatment of the problem.

3.1. *The Effect on Particle Velocities*

The particles in the disk are in circular motion with small-amplitude oscillations about their guiding centers. In the frame of the guiding center of a particle its motion is analogous to that of a three-dimensional harmonic oscillator. Therefore, we may expect the response of each particle to resemble that of a forced oscillator in classical mechanics.

We first plot the radial velocity component, v_R, as a function of radius R at four different times (Fig. 3), for particles with an initial random velocity of ~10 km s^{-1}. From these figures it is seen that the spread in the radial velocities increases dramatically with time.

An important quantity to look at is the change in the velocities of particles relative to their initial circular velocity. We define a quantity

$$v_{pc}^2 = [v_R^2 + (v_\varphi - v_c)^2]$$

as an estimate of planar random velocities relative to the circular velocity. We then calculate a quantity $\sigma_{pc\varphi}^2$ which is v_{pc}^2 averaged over all particles originally at a particular radius and with different azimuthal phases, $\sigma_{pc\varphi}^2 = \langle v_{pc}^2 \rangle_\varphi$. The subscript c serves as a reminder that this random planar velocity is relative to the original circular velocity. In Figure 4 we plot $\sigma_{pc\varphi}$ as a function of time for particles with five different initial velocities. The three frames show the behavior at three different radii.

A visually obtained estimate of the average value of $\sigma_{pc\varphi}$ at $T > 5 \times 10^8$ yr is used as a measure of the final random velocity of particles in further analysis. The strength of the tidal field increases rapidly over a few times 10^8 yr as seen from the rise time for the velocity in Figure 4.

The dependence of the particle response on the initial velocity amplitudes is as follows. At the smallest radius of 8.0 kpc (Fig. 4, *top*), the effect of the tidal field on the random velocities of particles is negligible. At an intermediate radius of 14 kpc (Fig. 4, *middle*), the perturbation amplitude is comparable to the initial oscillation amplitude of the high-velocity stars (~25–35 km s^{-1}) and the response of these particles is dependent on the initial amplitude of oscillation. For the colder components, with initial velocities ($\leq$17.5 km s^{-1}), the response is independent of the initial amplitude since the perturbation is far greater than the initial oscillation amplitude. At larger radii the final amplitude of all particles is dependent only on the forcing amplitude. This is clearly so at 20 kpc (Fig. 4, *bottom*) where the tidal forces are large. This behavior broadly resembles the response of an oscillator to forcing of different strengths. In Table 2 the final average values of $\sigma_{pc\varphi}$ are tabulated at three different radii for the "standard parameters" and a parallel disk for the logarithmic potential in equation (2) as well as the three-component potential discussed in § 3.3. The first three columns in this table serve as a comparison with tables that follow.

TABLE 2

PLANAR VELOCITY FOR STANDARD PARAMETERS

INITIAL $\sigma_{pc\varphi}$ (km s^{-1})	FINAL $\sigma_{pc\varphi}$ (km s^{-1})					
	Flattened Log Potential			Three-Component Potential		
	$R = 8^a$	$R = 14$	$R = 20$	$R = 8$	$R = 14$	$R = 20$
5.0.....	12.0	45.0	79.0	7.5	25.0	63.0
8.5.....	13.5	45.0	79.0	10.0	29.0	63.0
17.5.....	21.5	45.5	85.0	17.5	31.0	65.0
26.0.....	30.5	48.5	88.0	34.0	36.0	65.0
35.0.....	35.0	55.0	88.5	36.0	49.0	85.0

[a] Radius in disk in kpc.

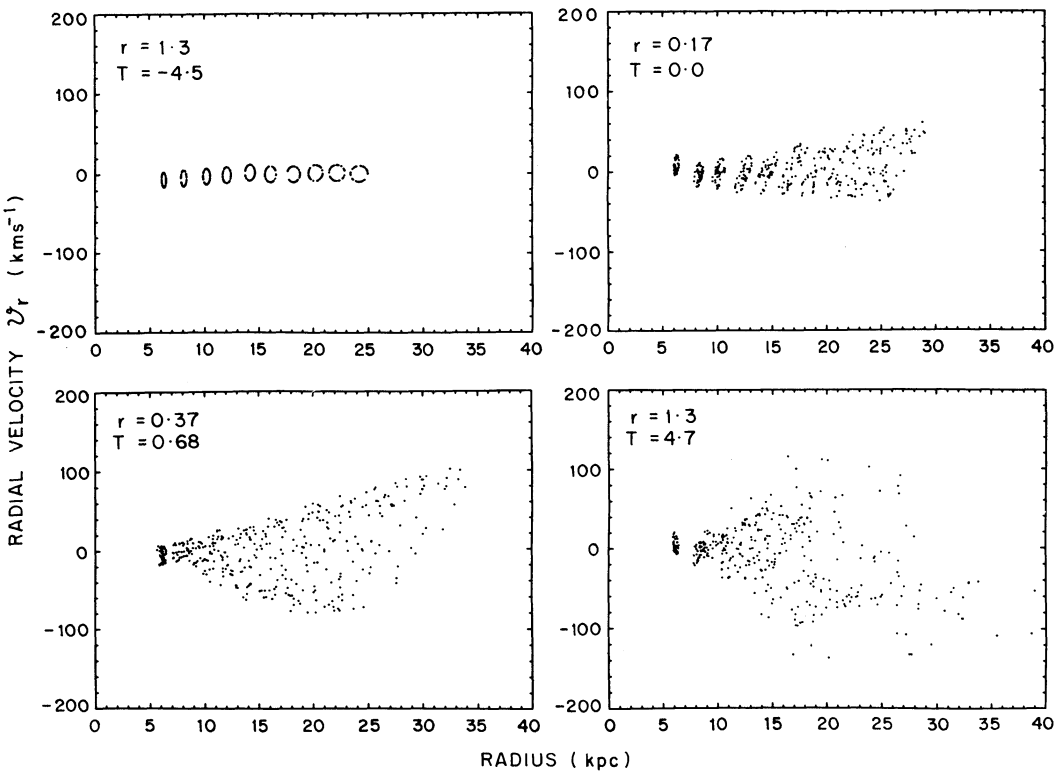

FIG. 3.—Radial velocities, v_R, of particles with initial radial velocities of 10 km s^{-1} plotted against their radii R. Successive frames give snapshots at four different points in the orbit through the cluster: T is time in 10^8 yr from closest approach, and r in Mpc, the distance from the cluster center. Data plotted for "standard parameters."

The time scale over which the perturbation acts is $\tau_{enc} \sim 3 \times 10^8$ yr. The time-dependent tidal force can be written as a Fourier series with the dominant frequency $\sim 2\pi/\tau_{enc}$. Thus a resonance between the epicyclic frequency and the dominant "frequency" of the tidal force is probably responsible for the large energy input to planar velocities. The vertical oscillation frequency is higher than the "forcing frequency" and no resonance occurs. That is to say that the external perturbation varies adiabatically over a vertical oscillation period. Consequently the system will evolve to one with a highly anisotropic velocity distribution. The dynamical consequences of a highly anisotropic velocity distribution on the stability of a disk are discussed in § 4.1.

From this we may conclude that at most radii within which molecular gas clouds are found ($\leq$14 kpc), the hotter stellar components will be relatively less affected than the colder gas components.

In Table 3, a comparison is made between the effects on particles in disks with different asymptotic circular velocities. Dwarf irregular galaxies frequently have rotation velocities of 70–100 km s^{-1}. Massive late-type spirals on the other hand can have $v_c \sim 300$ km s^{-1} (see Mihalas & Binney 1981). From this table it can be seen that particles in a disk with a small rotation velocity (100 km s^{-1}) experience a much larger increase in random velocities than those in a more rapidly rotating one. One reason for this is that the dynamical (rotation) time is greater for a slowly rotating disk than for a rapidly rotating one. Consequently the effects of the perturbation on a particle in the approaching phase of its orbit are not cancelled by the effects during its receding phase, as they would be if the particle was rotating rapidly. The effects of the perturbation are therefore seen much closer to the center of the galaxy when the rotation velocity is smaller. The dependence of the final random velocity of particles on the initial velocity of oscillation (Fig. 4) and on the rotation velocity is also an illustration of the fact that hotter stellar components are less affected than the colder components.

We now investigate the dependence on disk inclination, orbital parameters, and cluster parameters. Table 4 illustrates how the average value of $\sigma_{pc\varphi}$ long after the encounter depends on the inclination of the disk to the orbital plane. $\sigma_{pc\varphi}$ is given at three different radii, and for five different initial velocity amplitudes from 5 to 35 km s^{-1}. These numbers are extracted from velocity-time curves like those in Figure 4. From this table and Table 2 it is evident that the effect on the velocities is strongest when the disk plane is parallel to the orbital plane.

TABLE 3

DEPENDENCE ON ROTATION VELOCITY

INITIAL $\sigma_{pc\varphi}$ (km s^{-1})	FINAL $\sigma_{pc\varphi}$ (km s^{-1})					
	v_c[a] = 100 km s^{-1}			v_c = 300 km s^{-1}		
	R = 8[b]	R = 14	R = 20	R = 8	R = 14	R = 20
5.0.....	15.5	50.0	88.0	4.5	15.5	46.0
8.5.....	18.5	50.0	88.0	8.5	18.0	46.0
17.5.....	19.0	55.5	88.5	17.3	22.5	46.0
26.0.....	37.5	55.5	106.0	26.0	26.0	46.0
35.0.....	45.5	65.0	113.0	35.0	39.5	65.0

[a] Rotation velocity.

[b] Radius in disk in kiloparsecs.

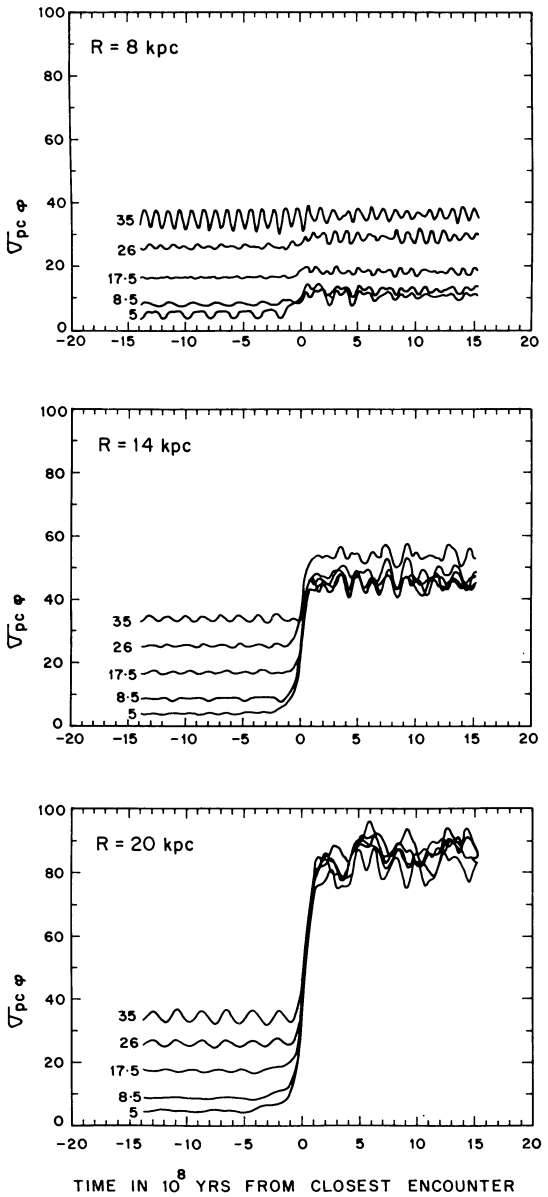

FIG. 4.—Planar velocity $\sigma_{pc\varphi}$ averaged over particles at all azimuthal phase points at the same radius, plotted as a function of time from closest approach. Figures plotted for three initial radii; in each figure $\sigma_{pc\varphi}$ is plotted for five initial planar random velocities: 5, 8.5, 17.5, 26, and 35 km s^{-1}.

Table 5 gives $\sigma_{pc\varphi}$ as in the previous table for five different orbits of the galaxy in a cluster with $a = 250$ kpc and $\sigma_{cl} = 1000$ km s^{-1}. All five orbits have the same total energy E but different angular momenta, and consequently different impact parameters. For four of these orbits, the rotation of the disk (when parallel to the orbital plane) is prograde and for the fifth it is retrograde ($L = -2.5$). As expected the effect on the particle velocities in a galaxy on the (prograde) orbit with the smallest impact parameter ($\sim 0.42a$ for $E = -1.5$, $L = 1.6$) is much greater than the effect on those which are on more circular orbits. The disk on the retrograde orbit is relatively unaffected by the encounter. This is in agreement with the work by Jefferys (1974). In Table 6 a comparison is made between different cluster potentials. For most cases studied we keep a fixed at 250 kpc, while σ_{cl} is varied. Simulations were performed for $\sigma_{cl} = 550$ km s^{-1} (case C1: e.g., A262), $\sigma_{cl} = 750$ km s^{-1} (case C2: e.g., A1367 and Virgo Cluster), $\sigma_{cl} = 1000$ km s^{-1} (case C3: e.g., Coma Cluster [also Table 2]) $\sigma_{cl} = 1250$ km s^{-1} (case C4: purely for illustration). We have also run one simulation for $\sigma_{cl} = 1500$ km s^{-1} (case C5) which is a much higher value than observed in nearby clusters but appears typical of some of the high-redshift Butcher-Oemler clusters (Butcher & Oemler 1978; Gunn 1989). These clusters will be discussed in § 4. The effects of the tidal field on the disk are negligible for the case when $\sigma_{cl} = 550$ km s^{-1}, and the results are not shown. The numbers in this table show that the heating of disk stars increase with the depth of the potential and disk galaxies in rich clusters would be the most severely affected.

The last three columns in Table 6 are case C6: $a = 100\ h_{50}^{-1}$ kpc and $\sigma_{cl} = 1000$ km s^{-1} and an orbit with $E = -1.5$ and $L = 5.5$. These orbital parameters were chosen to ensure that the pericenter is greater than 5 galaxy radii from the cluster center. This is to study the effects of a small cluster core radius deduced from gravitational lensing studies (Tyson et al. 1990). These values are to be compared with the final three columns of Table 2 since that orbit has the same impact parameter. The numbers in these columns imply that the tidal force would significantly perturb the planar random velocities of disk particles. The effect on the particles at large radii is sufficient to completely destroy the disk structure of the galaxy in such an encounter. This may be relevant to the conclusions of Whitmore (1990) that the fraction of S0 and spiral galaxies drop dramatically in the inner 100 kpc of most rich clusters.

To summarize, a galaxy in a rich cluster whose orbit carries it to within 250 kpc of the center experiences a large increase in planar random velocities of all particles at radii ≥ 14 kpc. Collisional dissipation between clouds will ensure that the

TABLE 4

DEPENDENCE ON DISK ORIENTATION

Initial $\sigma_{pc\varphi}$ (km s^{-1})	Final $\sigma_{pc\varphi}$ (km s^{-1})								
	Perpendicular (edge-on)			Perpendicular (face-on)			Inclined (45°)		
	$R = 8$[a]	$R = 14$	$R = 20$	$R = 8$	$R = 14$	$R = 20$	$R = 8$	$R = 14$	$R = 20$
5.0.....	9.0	22.0	42.0	5.0	10.0	25.0	5.0	18.0	36.0
8.5.....	11.0	23.0	45.0	8.5	11.0	25.0	8.5	19.0	36.0
17.5.....	18.0	38.0	45.0	17.5	20.0	30.0	17.5	21.0	40.0
26.0.....	26.0	38.0	47.0	26.0	30.0	35.0	26.0	30.0	43.0
35.0.....	35.0	42.0	60.0	35.0	39.0	50.0	35.0	41.0	54.0

[a] Radius in disk in kpc.

TABLE 5

DEPENDENCE ON ORBITAL PARAMETERS

Initial $\sigma_{pc\varphi}$ (km s^{-1})	Final $\sigma_{pc\varphi}$ (km s^{-1})											
	$L = 1.6$[a]			$L = 3.5$			$L = 5.0$			$L = -2.5$		
	$R = 8$[b]	$R = 14$	$R = 20$	$R = 8$	$R = 14$	$R = 20$	$R = 8$	$R = 14$	$R = 20$	$R = 8$	$R = 14$	$R = 20$
5.0.....	12.0	50.0	85.5	4.5	13.5	39.0	4.5	4.5	13.5	4.5	6.0	14.0
8.5.....	14.0	50.0	85.5	8.5	15.0	41.0	8.5	8.5	17.5	8.5	12.5	14.5
17.5.....	18.0	50.5	85.5	18.0	19.0	46.5	18.0	18.0	21.5	18.0	17.5	22.5
26.0.....	26.0	53.5	88.5	26.0	29.5	46.5	26.0	26.0	28.0	26.0	26.0	26.0
35.0.....	38.0	58.5	92.0	35.0	35.5	46.0	35.0	35.0	38.5	35.0	35.5	35.5

[a] Angular momentum.
[b] Radius in disk.

cloud random velocities never really attain such high values and these numbers are indicative of the energy injected into the system. The nondissipative stellar component develops an anisotropic velocity dispersion as a result of the encounter.

3.2. *Effects on the Spatial Distribution of Particles*

The evolution of the spatial distribution of test particles is studied as the galaxy traverses the cluster. Particles are originally placed on concentric circles at equally spaced radii between 6 and 24 kpc and at equally spaced azimuthal (φ) phases. They have z-scale heights ≤ 550 pc determined by the amplitude of the vertical oscillation velocity. The distribution is evolved for particles with five different initial velocity amplitudes. The central 6 kpc region is not studied because the tidal field is already fairly weak at 8 kpc, and since there are no gravitational interactions between particles most effects in the inner region will not be reproduced (see, for example, Toomre & Toomre 1972). This region should, however, be studied with an N-body code for completeness.

The evolution of the particle distribution in the disk is influenced primarily by the inclination of the disk to the orbital plane. The effects on the particle distribution are studied for disks of different inclinations for the "standard parameters"; i.e., $a = 250$ kpc, $\sigma_{cl} = 1000$ km s^{-1}, and $E = -1.5$, $L = 2.5$.

When the plane of the disk is parallel to the orbital plane (Fig. 5), a transient two-armed spiral pattern begins to form after the galaxy passes pericenter ($T = 0.0$). This pattern winds up in $\sim 1.5 \times 10^8$ yr. The formation of the spiral pattern is due to the cos $2(\psi - \varphi)$ dependence in the "tidal potential" (eq. [11]). The time taken for the galaxy to cross the core region is of the order of the rotation time in the disk (a few times 10^8 yr). Thus the nonaxisymmetric tidal perturbation has a "pattern frequency," Ω_p, which is comparable to the rotation frequency, Ω at ~ 10 kpc. Circular orbits have resonant frequencies at $\Omega_p = \Omega$ and $\Omega_p = \Omega \pm \kappa/2$. This results in an enhancement of the weak kinematic spiral wave which lasts the duration of the encounter (Kalnajs 1973). In the final distribution of particles (at $T \geq 10^9$ yr)., a small fraction of particles are transported out to radii of up to 1.5–2.0 times that of the original radius of the disk. The effect on the z-distribution of particles is negligible.

Figures 6 and 7 are face-on views of the disk when it is inclined at different angles to the orbital plane. For all other inclinations of the disk the major effect on the particle distribution is that the circular disk is compressed by the tidal field as it passes through the cluster core and reexpands to ~ 1.5 times the original size thereafter.

When the disk is perpendicular and face-on at pericenter, the tidal forces in the plane are predominantly due to the components T_{x_2} and T_{x_3} (eq. [8]). Since these components are nearly equal during the core crossing, the compression is more or less axisymmetric and the disk remains circular throughout the compression and subsequent expansion (Fig. 6).

When the disk is perpendicular and edge-on at pericenter, the tidal forces in the plane are T_{x_1} and T_{x_3}, and the compression is nonaxisymmetric and the circular disk is deformed to a

TABLE 6

DEPENDENCE ON CLUSTER POTENTIAL

Initial $\sigma_{pc\varphi}$ (km s^{-1})	Final $\sigma_{pc\varphi}$ (km s^{-1})											
	C2[a]			C4			C5			C6		
	$R = 8$[b]	$R = 14$	$R = 20$	$R = 8$	$R = 14$	$R = 20$	$R = 8$	$R = 14$	$R = 20$	$R = 8$	$R = 14$	$R = 20$
5.0.....	5.0	12.5	36.0	15.0	54.5	100.0	35.0	79.5	113.0	11.0	70.0	168.0
8.5.....	8.5	12.5	37.5	17.5	56.0	100.0	35.5	90.0	113.0	12.5	75.0	196.0
17.5.....	17.5	22.0	43.0	23.0	60.0	103.5	36.5	90.0	113.5	17.5	80.0	215.0
26.0.....	26.0	26.0	47.0	32.0	62.0	105.0	40.0	90.0	128.5	28.0	90.0	221.0
35.0.....	35.0	40.0	52.0	42.0	76.0	105.0	40.0	106.0	135.5	39.0	90.0	230.0

[a] Cluster Parameters:
C2: $a = 250$ kpc, $\sigma_{cl} = 750$ km s^{-1};
C3: $a = 250$ kpc, $\sigma_{cl} = 1000$ km s^{-1} (Table 2);
C4: $a = 250$ kpc, $\sigma_{cl} = 1250$ km s^{-1};
C5: $a = 250$ kpc, $\sigma_{cl} = 1500$ km s^{-1};
C6: $a = 100$ kpc, $\sigma_{cl} = 1000$ km s^{-1}.
[b] Radius in kpc.

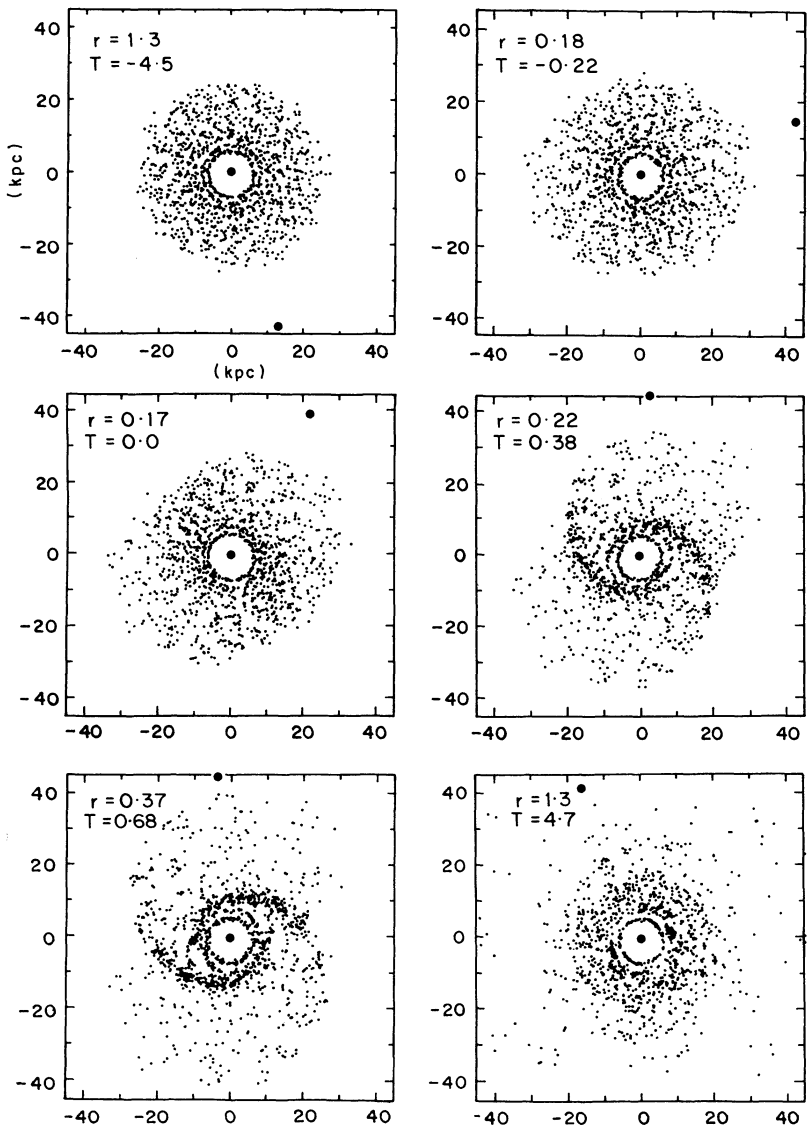

FIG. 5.—Face-on view of disk galaxy at different points in the orbit; r and T as in Fig. 3. The disk is parallel to the orbital plane. In each frame an imaginary arrow joining the points marked (⊕) indicates the direction to the cluster center. Scale on axes in kiloparsecs.

compressed oval-like distribution (Fig. 7). In both these cases the vertical distribution of the disk particles is unaffected.

A disk with its plane inclined at 45° to the orbital plane is also transiently compressed into an ellipse as it passes through the central core. Figure 8 is an edge-on view of the disk for this orientation: a weak transient warp is seen in the plane of the disk as the galaxy passes pericenter. In this figure only the cold components (5–10 km s^{-1}) are plotted. The vertical displacement of the midplane for this set of parameters at $R \sim 20$ kpc is ~350 pc. No warp is seen in the hotter stellar components. This is the only case where the z-distribution of particles is affected by the encounter. This occurs because of a signficant component of the tidal force normal to the plane of the disk is introduced by the inclination to the orbital plane. The warp is kinematic and in the absence of self-gravity, phase-mixing effects rapidly wash it out (last frame in Fig. 8).

The qualitative behavior of the particle distribution is determined primarily by the inclination of the disk. Changing the cluster's velocity dispersion and the galaxy's orbital parameters results in qualitative changes to the distribution. These changes may be summarized as follows.

Galaxies on orbits with smaller pericenters (smaller L) experience stronger effects on their particle distributions than those which undergo distant encounters. Similarly, the tidal field of a deeper cluster potential ($\sigma_{cl} = 1250$–1500 km s^{-1}) affects the distribution more strongly than a shallower potential ($\sigma_{cl} = 750$ km s^{-1}). By this we mean that the spiral pattern formed is stronger, and the degree of compression is greater than for distant encounters and shallow potentials. For a galaxy in a very rich potential ($\sigma_{cl} \sim 1200$ km s^{-1}) and on an orbit with $L \leq 2.5$ (pericenter ≤ 170 kpc), the average surface area of the disk (when seen face-on) decreases by a factor as high as 2 due to the compression.

For case C6 (smaller cluster core radius) the effects on the particle distribution are quite different. The tidal field is very strong and the disruptive radial component causes a disk parallel to the orbital plane to expand to about twice its initial radius. The spiral feature is almost insignificant. When the disk

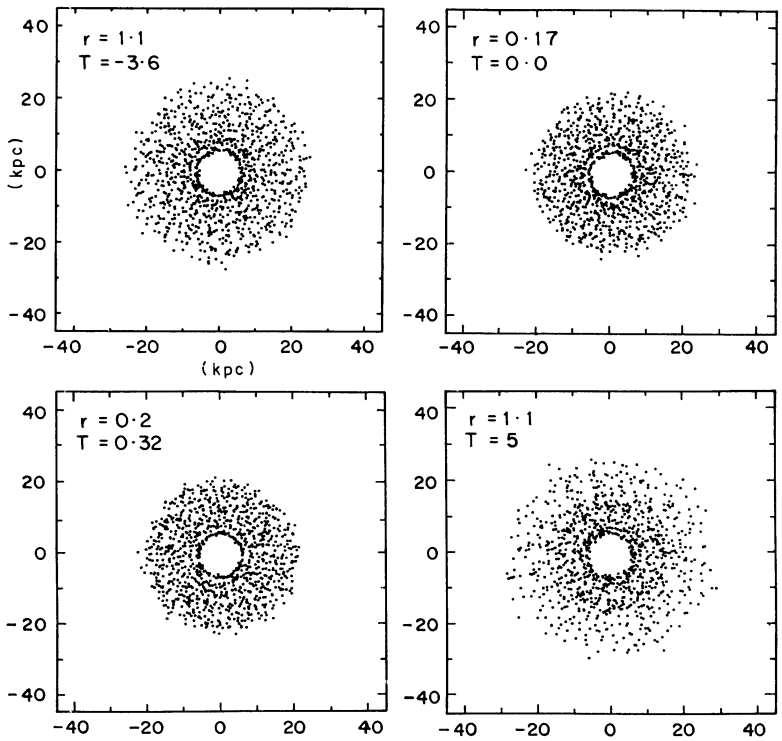

FIG. 6.—Same as in Fig. 5 for a disk with plane perpendicular to orbital plane and seen face-on at pericenter

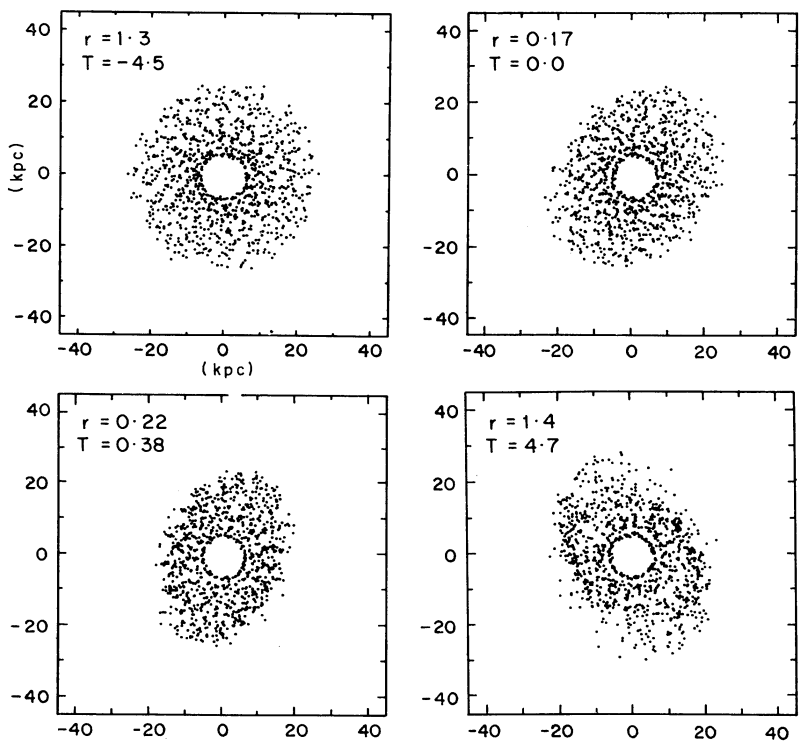

FIG. 7.—Same as in Fig. 5 for a disk with plane perpendicular to orbital plane and seen edge-on at pericenter

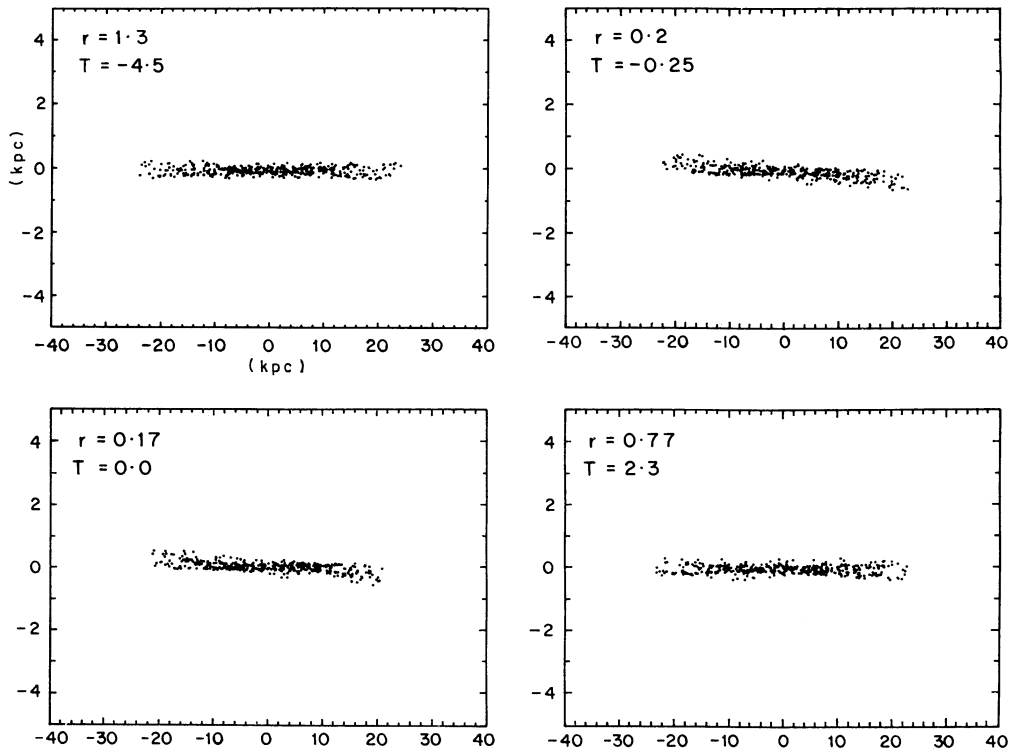

FIG. 8.—Edge-on view of galaxy for a disk with plane inclined at 45° to orbital plane. The scales on the two axes have been made unequal to highlight the slight warp in the disk.

is inclined to the orbital plane, as expected, the warping of the disk is extremely strong—so strong in fact that at the end of the encounter the disk structure is almost completely destroyed due to very large out-of-the-plane motions and velocities ($\langle v_z^2 \rangle^{1/2} \sim 60$–$90$ km s^{-1}). The face-on view of the disk again undergoes strong oval compression. It may be concluded that the disk would probably be disrupted within a few crossings. It is therefore of extremely great importance to determine whether the lensing data on the core radii of clusters gives the core radius of the dark matter distribution of the cluster or simply some effective core radius which is small due to the presence of a massive cD galaxy at the cluster center.

3.3. *Effect of the Dark Matter Halo*

The results discussed so far have been for a highly flattened disk galaxy with a logarithmic potential (§ 2). Real disks are believed to have massive dark matter halos. Since the stars and gas stay predominantly in the plane of the disk, it may be argued that the presence of the halo is unlikely to affect their behavior very strongly. However, the halo itself extends to much larger radii than the stellar component and is likely to be tidally stripped (Merritt 1984).

Most mass models produced to fit observed rotation curves require three components: a spheroidal nucleus, a disk, and a halo. Miyamoto & Nagai (1975) suggested a potential-density pair whose light distribution can be made to fit that of spirals quite nicely. An improved version with three components (Miyamoto et al. 1980) gives a rotation curve which provides a good fit to that of our Galaxy and stays flat out to 50 kpc. The potential suggested by them is

$$\Phi_g = -\sum_i^3 \frac{GM_i}{[R^2 + (a_i + \sqrt{z^2 + b_i^2})^2]^{1/2}},$$

where M_i are the masses of the three components and a_i and b_i are scale lengths. Their galaxy has a rather high total mass of $9.1 \times 10^{11}\ M_\odot$ with $M_1 = 0.195 \times 10^{11}\ M_\odot$, $M_2 = 1.74 \times 10^{11}\ M_\odot$, $M_3 = 7.35 \times 10^{11}\ M_\odot$. The scale lengths are $a_1 = 0.0$, $a_2 = 6.2$ kpc, $a_3 = 0.0$, $b_1 = 0.47$ kpc, $b_2 = 0.15$ kpc, and $b_3 = 31.2$ kpc. The potential, however, has a force normal to the plane (frequently referred to as the K_z law) which is stronger than the one observed by Oort for stars in the solar neighborhood.

We have evolved the particle distribution in this galaxy for the "standard parameters" and the final planar random velocities are given alongside those for the logarithmic potential in Table 2. A disk parallel to the orbital plane develops a two-armed spiral as in Figure 5. Disks with other orientations are compressed nonaxisymmetrically as in Figure 7. The vertical distributions and velocities of particles are unaffected in all cases except when the disk is inclined to the orbital plane. The plane of the disk is more strongly warped, especially at large radii. The vertical thickness of the plane increases especially at large radii, almost doubling at the end of the encounter.

Sparke & Casertano (1988) have shown that the presence of a triaxial halo potential whose axis is inclined to the rotation axis of the disk will produce long-lived dynamical warps in the disk. The warp here can also be thought of as a consequence of an interaction between a fictitious "ellipsoidal tidal potential" centered on the galaxy and the inclined disk potential.

Since the particles we have considered have fairly limited vertical oscillation amplitudes, the disk potential dominates their dynamics and it is therefore not surprising that the dark halo has little effect on their dynamics except at large radii. The most general case would be one in which the disk was inclined to the orbital plane and warped disks may be an observable signature of the tidal interaction.

4. DISCUSSION: DYNAMICAL CONSEQUENCES

In this model the particles in the galaxy do not interact gravitationally and hence the effects of the perturbations on the subsequent dynamics of the system cannot be studied. Nonetheless, an understanding of the behavior of these systems in the absence of self-gravity enables us to postulate possible dynamical consequences for a system of gravitating particles.

Here some dynamical consequences of increasing the planar velocity dispersion of particles are suggested. Also discussed is the effect of the nonaxisymmetric perturbation and the increased frequency of cloud collisions in the disk on its subsequent evolution. The discussions are based on general qualitative arguments and need to be confirmed by a detailed numerical study.

4.1. *Fire-Hose Instability in the Disk*

Kulsrud, Mark, & Caruso (1971) and Toomre (1966) have shown that a flattened stellar system, in which the velocity dispersion in the plane is much greater than that perpendicular to it, will develop a bending instability (Kulsrud et al. 1971), similar to the "fire-hose" instability in a neutral plasma. Raha et al. (1991) have shown that an N-body stellar disk which forms a bar at its center will soon undergo an out-of-plane bending instability which disrupts the bar. After the onset of bending, the bar quickly evolves into a peanut-shaped bulge and the thickness of the disk increases. They attribute the bending modes to a fire-hose instability which sets in due to the velocity anisotropy which results due to streaming motions around the bar. It has been found that a stellar disk becomes unstable to the fire-hose instability if the ratio of σ_x the horizontal velocity dispersion to σ_z the vertical velocity dispersion is greater than 3 (Toomre 1966 and Raha et al. 1991).

Real stellar disks do not have very anisotropic velocity dispersions so this instability is mainly of academic interest. For the Galaxy the ratio of the radial velocity dispersion σ_r to the vertical velocity dispersion σ_z is ≤ 2.0 for all components (Mihalas & Binney 1981). The planar velocity dispersion σ_p is $(3/2)^{1/2}\sigma_r$ (because $\sigma_\varphi^2 \sim 1/2\sigma_r^2$). An average value for the ratio $\sigma_p/\sigma_z \sim 1.5^{3/2}$ in an equilibrium disk.

In § 3.1 it was shown that the planar velocity dispersion of stars increases to 50–70 km s^{-1} for strong tidal fields. The late-type stars (G–M) which represent the mass in the disk that provides the gravitational restoring force against the instability have $\sigma_z \sim 15$ km s^{-1}. This will result in a ratio of (σ_p/σ_z) of ~ 3.5–4.5 for these stars after the tidal encounter. These ratios are above the threshold level for stability (≥ 3) and the disk is expected to become unstable to the fire-hose instability.

This bending instability will rapidly convert the planar kinetic energy of the particles to kinetic energy of z-motion. We assume that the system evolves to an equilibrium where the final velocity dispersion ratio (σ_p/σ_z) is similar to its value in an equilibrium disk (~ 1.5). Since we can assume that energy is conserved at times ($T > 5 \times 10^8$ yr), a simplistic estimate of the resultant thickening of the disk can be made.

In obtaining this estimate we do not take into account the fact that the degree of anisotropy varies over the disk. A similar situation existed in the numerical simulations of Raha et al. and the local treatment was found to be applicable to a large extent. The local approximation is applicable if the growth rate of the instability is larger than the rotation frequency at that radius.

For the purpose of this calculation it is assumed that the disk is an infinite thin sheet both before the instability and after the subsequent relaxation to equilibrium. In the thin disk approximation the z-displacement is $z(t) = z_0 \cos(\nu t + \alpha)$ (as in § 2.4), where z_0 is the amplitude of vertical oscillation. The total energy is given by

$$E = \tfrac{1}{2}[\langle v_p^2\rangle + \langle v_z^2\rangle] + \langle \Phi_z\rangle .$$

Since $\langle v_z^2\rangle = (1/2)\nu^2 z_0^2$ and the average z-potential energy, $\langle \Phi_z\rangle = (1/2)\nu^2 z_0^2$, we get the total energy

$$E = \tfrac{1}{2}\langle v_p^2\rangle + \tfrac{3}{4}\nu^2\langle z_0^2\rangle . \tag{13}$$

In the thin disk approximation, the frequency of z-oscillation $\nu^2 = 4\pi G\Sigma_0$ where, Σ_0, the average surface density of the disk does not change. We approximate $\sigma_p \sim \langle v_p^2\rangle^{1/2}$ and $\sigma_z \sim \langle v_z^2\rangle^{1/2}$. Quantities just before the onset of instability and after equilibrium are noted by the subscripts i and e, respectively. The ratios of the planar to vertical velocity dispersions are given by

$$\frac{\sigma_{pi}}{\sigma_{zi}} = c_i , \qquad \frac{\sigma_{pe}}{\sigma_{ze}} = c_e = (1.5)^{3/2} . \tag{14}$$

Substituting for σ_{pi}, and σ_{pe} above, we get

$$E_i = \tfrac{1}{2}c_i^2\sigma_{zi}^2 + \tfrac{3}{4}\nu^2\langle z_{0i}^2\rangle ,$$

$$E_e = \tfrac{1}{2}c_e^2\sigma_{ze}^2 + \tfrac{3}{4}\nu^2\langle z_{0e}^2\rangle .$$

Since there is no dissipation in the stellar component we can assume that total energy after the encounter is conserved ($E_i = E_e$), This gives a relation between the mean thickness of the disk before the instability sets in, $\langle z_{0i}^2\rangle^{1/2}$, and its thickness after it returns to equilibrium, $\langle z_{0e}^2\rangle^{1/2}$,

$$\frac{\langle z_{0e}^2\rangle}{\langle z_{0i}^2\rangle} = \left[\frac{c_i^2 + 3}{c_e^2 + 3}\right] . \tag{15}$$

In a Coma-like cluster the values of $c_i \sim 3.5$–4.5. This results in only a small increase in disk thickness by a factor of 1.5–1.9. However, in a deep cluster with a velocity dispersion $\sigma_{cl} \sim 1500$ km s^{-1} (the Butcher-Oemler cluster example in Table 6) $c_i \sim 5.5$–6.0. Galaxies in such a cluster would become a factor of 2.3–2.5 times thicker after a passage through the core of the cluster.

Thus strong cluster tidal fields (either due to a deep potential or a small core radius) can cause a thickening of the disks of spiral galaxies. Burstein (1979) has observed the thick disk components of a number of S0 galaxies and finds them to be a factor of ~ 2.0–2.5 times thicker than their thin disk components. This supports the hypothesis that the active galaxies in the Butcher-Oemler clusters are the progenitors of S0 galaxies.

4.2. *Gas Infall and Starbursts*

Lynden-Bell & Kalnajs (1972) showed that a nonaxisymmetric spiral perturbation can transport angular momentum in a stellar disk. If the spiral pattern is trailing, angular momentum will be transported outward. In the simulations (§ 3.2), a trailing spiral pattern was formed for certain orientations of the disk (Fig. 5). It is, therefore, reasonable to expect angular momentum transport to occur. It can be shown that an elliptical perturbation of the kind produced in the simulations (Fig. 7) can also transport angular momentum (Valluri 1993).

As discussed in § 3.1 the random velocities of clouds in the

disk were found to increase by a factor of ~5–10. This will result in a higher cloud collision frequency and these inelastic collisions will result in a dissipation of the kinetic energy of the clouds. A combination of angular momentum transport and dissipation can cause infall of gas to the center and enhance the rate of nuclear star formation. A similar scenario has been discussed in considerable detail by Norman (1987) and Icke (1985) in the context of starburst galaxies. In a cluster galaxy the infall rate and activity are likely to be less dramatic than in the case of galaxy-galaxy interactions. The N-body simulations of Byrd & Valtonen (1990) indicate that gas infall to the center of a disk galaxy occurs with rates as high as 1 $M_\odot$ yr^{-1}.

It has been recently observed (Canzian & Scoville 1991) that several noninteracting spiral galaxies in the Virgo Cluster have unusually large amounts of molecular gas within 5 kpc of their centers. Tidal fields in the Virgo Cluster are not very strong (Table 6) but a moderate rate of gas infall to the centers of galaxies in this cluster may be expected. These observations of the central molecular gas excess are well explained by the mechanisms proposed here. Some of these galaxies also show evidence of excess star formation and nuclear activity (Cayatte et al. 1990). This is the nearest cluster and hence it is the only one for which such observations are available. It is hoped that more observations of rich clusters will confirm the predictions made here.

There is substantial evidence to show that a large fraction of spiral galaxies (>25%) in rich clusters at redshifts of 0.3–0.5 shows evidence of a recent starburst or Seyfert-like nuclear activity (see Gunn 1989 for a review, Butcher & Oemler 1978). These Butcher-Oemler clusters frequently have extremely high line-of-sight velocity dispersions (e.g., $\sigma_{cl} = 1500$ km s^{-1} in Cl 0016+16 and as high as $\sigma_{cl} = 3000$ km s^{-1} in 3C 295) which are probably indicative of deep cluster potentials or a cluster which is forming (and possibly undergoing virialization) by the merger of subclusters (Schindler 1991). Some authors have argued that the tidal fields in rich clusters were stronger in the past, particularly during the epoch of cluster formation and violent relaxation (Gunn 1977; White & Rees 1978). This has also been emphasized by Merritt (1984) in the context of the evolution of the mass distribution in clusters due to tidal stripping by the cluster potential. There is also recent evidence from the evolution of the X-ray luminosity functions of clusters that a significant fraction of clusters are being formed by the mergers of groups between $z = 0.6$ and 0.3 (Henry et al. 1992).

If the results of our modeling of steady-state cluster potentials are any indication of real systems, we may expect that a disk galaxy within a rich cluster with a $\sigma_{cl} \sim 1500$ km s^{-1} would experience very strong tidal fields. The burst of activity in the galaxies in these clusters could have been induced by global tidal fields. This mechanism could act along with shock compression of the molecular clouds by the intracluster medium (ICM) (Dressler & Gunn 1983). Gunn (1989) has argued that the ram pressure of the ICM, though strong, is inadequate to produce the required amount of star formation to account for the blue light. He suggests that spiral galaxies must have been far more gas-rich in the past. While this is possible, it is likely that the ram pressure compression provided by cloud-cloud collision could account for a substantial mass of gas undergoing compression and collapse. Also the gas infall could trigger the observed nonstellar nuclear activity. If the tidal heating of both the stars and the gas is sufficiently strong a spiral galaxy would be converted into an S0 galaxy with a thick disk (§ 4.1) and very little gas. This would also explain why present-day, relaxed clusters tend to be rich in S0 galaxies, whereas poor, irregular clusters, which show no sign of relaxation, are spiral-rich.

5. SUMMARY

We have used the restricted three-body method to model the effect of the mean tidal field of a cluster of galaxies on the internal dynamics of a disk galaxy falling into it for the first time. We summarize the main results and conclusions below.

1. The tidal field increases the planar random velocities of particles in the disk. The colder gas components and early-type stars experience a relatively larger increase than the hotter stellar components. Slowly rotating disks are more strongly heated than rapidly rotating ones. The actual increase in the planar velocity dispersion depends strongly on the initial parameters. The z-velocity dispersion is almost unaffected by the tidal field. This results in an anisotropy between the planar and vertical random velocities of $\sigma_p/\sigma_z \geq 3$.

2. The evolution of the particle distribution is strongly influenced by the orientation of the plane of the disk to the orbital plane. A disk parallel to the orbital plane forms a transient two-armed spiral pattern. Disks perpendicular or inclined to the orbital plane are compressed either axisymmetrically or to an elliptical distribution. The z-distribution of particles is unaffected by the tidal field except in the case when the disk is inclined to the plane of the orbit, when a warp is seen in the low-velocity dispersion particles (5–10 km s^{-1}).

3. The effects on the spatial distribution of particles and on their random velocities depend on the orbit of the galaxy in the cluster: galaxies which are on orbits which pass closer to the cluster center are more strongly perturbed. Galaxies in deeper cluster potentials (high σ_{cl}) are perturbed more strongly than those in shallow potentials. If clusters have a small core radius of ~100 kpc as implied by recent gravitational lensing data, the tidal fields would be very much stronger and a disk galaxy passing within ~200 kpc of the center would probably be disrupted.

4. The effect of the tidal field on the planar motions of disk particles is not significantly altered by the presence of a large dark matter halo. However the vertical motions of the disk are influenced by the presence of a halo—the thickness of the disk is significantly increased at large radii, and the warping of the disk is more pronounced.

We have argued that the tidal interaction will have the following consequences on a realistic self-gravitating galaxy.

1. The strong velocity anisotropy is expected to make the disk unstable to the "fire-hose instability." This will lead to out-of-plane bending of the disk and is expected to result in the transfer of planar kinetic energy to kinetic energy of vertical motion. As a result the disk thickness will increase by a factor of ~2.0–2.5 for galaxies is the Butcher-Oemler–like clusters.

2. The formation of a nonaxisymmetric perturbation in the disk (either a spiral or elliptic perturbation) will lead to angular momentum transport. Dissipation of kinetic energy of the gas clouds is expected due to the increased frequency of cloud collisions. These two processes will together lead to gas infall to the center and subsequently, enhanced star formation.

3. It is proposed that tidal fields in clusters were stronger in the past when rich clusters were forming via mergers and undergoing (violent) relaxation. These tidal fields could have triggered active star formation in spiral galaxies. This could provide an additional mechanism for triggering activity in

infalling spiral galaxies (and "post starburst" galaxies) in the high redshift Butcher-Oemler clusters.

The computations were performed using several algorithms by Press et al. (1986) and the adaptive numerical integrator (ODEN) was written by Fred Clare of NCAR, Boulder, CO (based on an algorithm by F. Sampine & M. K. Gordon).

I would like to thank Chanda Jog, my thesis advisor, and Rajaram Nityananda for their advice and support throughout the course of this work. I am grateful to them for numerous suggestions and many useful discussions. I also wish to thank Ramanath Cowsik for many fruitful discussions, and for hospitality at the Tata Institute of Fundamental Research in 1991 July. I am grateful to the Raman Research Institute for permitting me the use of their computational facilities where a major portion of this work was carried out. I particularly wish to acknowledge the assistance of Rajashekar and Ramdurai of the RRI computer center. I am also grateful to Drs K. Indulekha, J. Ostriker, and T. Padmanabhan, for illuminating discussions and to Mousumi Das for reading the manuscript. I wish to thank the anonymous referee for detailed comments and suggestions which helped improve the paper. This work forms part of a Ph.D. thesis submitted to the Indian Institute of Science.

REFERENCES

Bahcall, N. A. 1975, ApJ, 198, 249
Binney, J., & Tremaine, S. 1987, in Galactic Dynamics (Princeton: Princeton Univ. Press) (BT)
Burstein, D. 1979, ApJ, 234, 829
Butcher, H., & Oemler, A. 1978, ApJ, 219, 18
Byrd, G., & Valtonen, M. 1990, ApJ, 350, 89
Canzian, B., & Scoville, N. 1991, BAAS, 23, 1369
Cayatte, V., van Gorkom, J. H., Balkowski, C., & Kotanyi, A. J. 1990, AJ, 100, 604
Cowsik, R., & Ghosh, P. 1987, ApJ, 317, 26
Dressler, A., & Gunn, J. E. 1983, ApJ, 270, 7
Giovanelli, R., & Haynes, M. P. 1985, ApJ, 292, 404
Gunn, J. E. 1977, ApJ, 218, 592
Gunn, J. E. 1989, in Epoch of Galaxy Formation, ed. C. S. Frenk et al. (Dordrecht: Kluwer), 167
Gunn, J. E., & Gott, J. R. 1972, ApJ, 176, 1
Haynes, M. P. 1988, in The Minnesota Lectures on Clusters of Galaxies and Large Scale Structure, ed. J. M. Dickey (ASP Conf. Ser. 5), 71
Henry, J. P., Gioia, I. M., Maccacaro, T., Morris, S. L., Stocke, J. T., & Wolter, A. 1992, ApJ, 386, 408
Huchra, J. 1984, in The Virgo Cluster, ed. O.-G. Richter & B. Binggeli (Garching: ESO), 181
Icke, V. 1985, A&A, 144, 115
Jefferys, W. H. 1974, AJ, 79, 710
Kalnajs, A. J. 1973, Proc. Astr. Soc. Australia, 2, 174
King, K. R. 1972, ApJ, 174, L123
Kulsrud, R. M., Mark, J. W.-K., & Caruso, A. 1971, Ap&SS, 14, 52
Lynden-Bell, D., & Kalnajs, A. J. 1972, MNRAS, 157, 1
Merritt, D. 1984, ApJ, 276, 26
Mihalas, D., & Binney, J. J. 1981, Galactic Astronomy (2nd ed.; San Francisco: Freeman)
Miller, R. H. 1988, Comm. Ap., 13, 1
Miller, R. H., & Smith, B. F. 1982, ApJ, 253, 58
Miyamoto, M., & Nagai, R. 1975, PASJ, 27, 533
Miyamoto, M., Satoh, C., & Ohashi, M. 1980, A&A, 90, 215
Norman, C. A. 1987, in Starburst and Galaxy Evolution, ed. T. X. Thuan, T. Montemerle, & J. T. Thanh Van (Gif sur Yvette: Ed. Frontiere), 483
Ostriker, J. P., Binney, J., & Saha, P. 1989, MNRAS, 241, 849
Ostriker, J. P., Spitzer, L., & Chevalier, R. A. 1971, ApJ, 176, L51
Press, W. H., Flannery, B. P., Teukolsky, S. A., & Vetterling, W. T. 1986, Numerical Recipes (Cambridge: Cambridge Univ. Press)
Raha, N., Sellwood, J. A., James, J. A., & Kahn, F. D. 1991, Nature, 352, 411
Sarazin, C. A. 1986, Rev. Mod. Phys. 58, 1
Schindler, S. 1991, in Traces of Primordial Structure in the Universe (MPE Rept. 227), ed. H. Böhringer & R. A. Treumann (Garching: Max-Plank-Institut für Extraterrestrische Physik), 155
Sparke, L. S., & Casertano, S. 1988, MNRAS, 234, 873
Tammann, G. A., & Binggeli, B. 1987, in High Redshift and Primeval Galaxies, ed. J. Bergeron et al. (Gif sur Yvette: Ed. Frontiere), 149
Toomre, A. 1966, in Notes from the Geophysical Fluid Dynamics Summer Program, Woods Hole Oceanographic Institute, 111
Toomre, A., & Toomre, J. 1972, ApJ, 178, 623
Tyson, J. A., Valdes, F., & Wenk, R. A. 1990, ApJ, 349, L1
Valluri, M. 1993, Ph.D. thesis, (Bangalore: Indian Institute of Science)
White, S. D. M., & Rees, M. J. 1978, MNRAS, 183, 341
Whitmore, B. C. 1990, in Clusters of Galaxies, STScI Workshop Proceedings, ed. M. J. Fitchett, W. Ogerele, & L. A. Danly (Cambridge: Cambridge Univ. Press), 139